Tungsten Densities from VUV and X-ray Spectroscopy

I. Faust, T. Pütterich, R. Dux, T. Odstrčil, M. Sertoli

Max Planck Institut für Plasmaphysik - Garching

June 13, 2018

ASDEX Upgrade

Tungsten line analyzed by UV and X-ray spectrometer correlation

- The Compact Soft X-ray spectrometer (CSXR) observes several tungsten lines in high T_e discharges
- Correlation to other tungsten (W) measurements used to characterize the brightest unknown line in wavelength range
- This new method of line characterization using the tungsten concentration determined its charge state (W^{45+})
- The line could be used for precise measurements of core tungsten density *profiles* (for several experiments with similar spectrometers)

The CSXR measures argon lines near .4 nm

- The CSXR is a crystal X-ray spectrometer (using spherically-bent quartz)
- It has high resolution of wavelengths between .39 and .4 nm
- 10ms time resolution useful for argon impurity studies
- CSXR absolute calibration determined by M. Sertoli

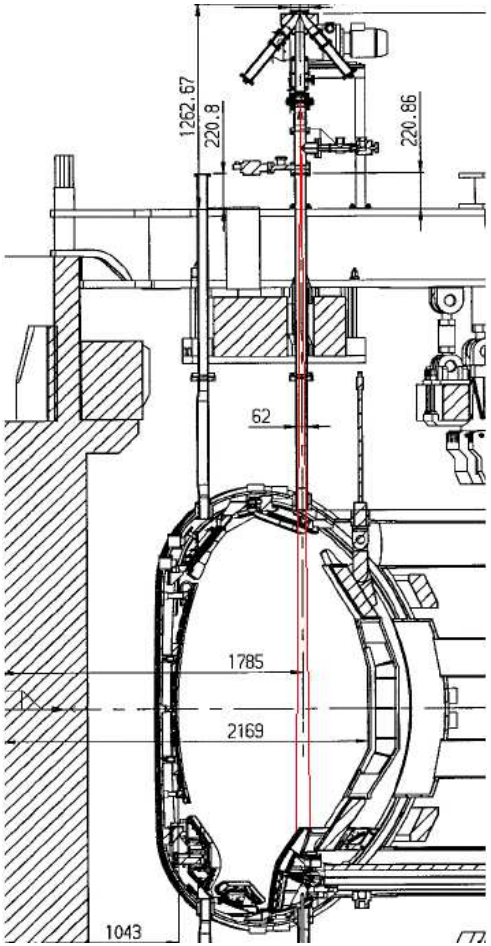

Geometry of the CSXR[1]

[1] Adapted from Sertoli's Thesis (LMU 2010)

Well-characterized He-like argon lines exist in CSXR wavelength range

- Four prominent Ar^{16+} lines exist in the .39-.4nm range (known as *W*, *X*, *Y*, and *Z*)
- Properties of these lines yield plasma conditions
  - Intensity ratio (X+Y)/Z $\propto n_e$
  - Line intensity $\propto n_i$
  - Line width $\propto T_i$
  - Line centroid $\propto v_i$
  - Satellite to W line ratio $\propto T_e$
- The Ar^{16+} charge state is dominant for T_e between .4 and 3 keV

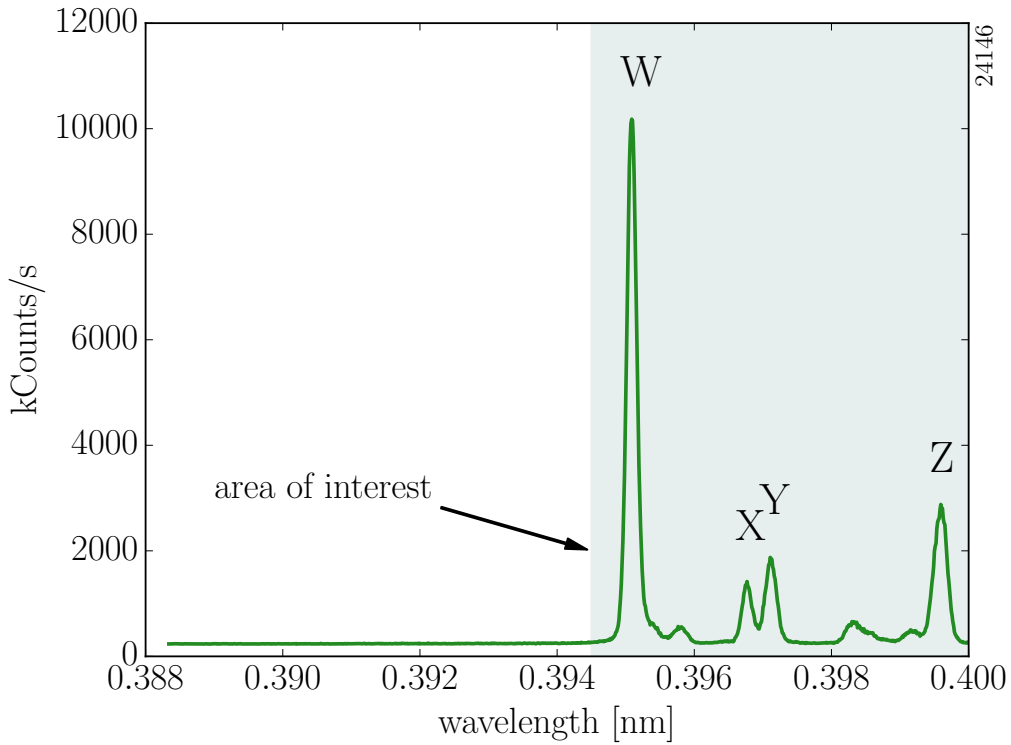

Imaging spectrometers used on other experiments for He-like Ar

- X-ray Imaging Crystal Spectrometers (XICS) developed by M. Bitter[1] and PPPL
- XICS systems have been implemented on several tokamaks/stellarators
  - NSTX-U
  - W-7X
  - EAST
  - *formerly* C-Mod
- These systems all measure He-like Ar lines (*i.e.* W, X, Y, and Z)
- Edge XICS-system to be built by India for ITER (not .39-.4 nm)

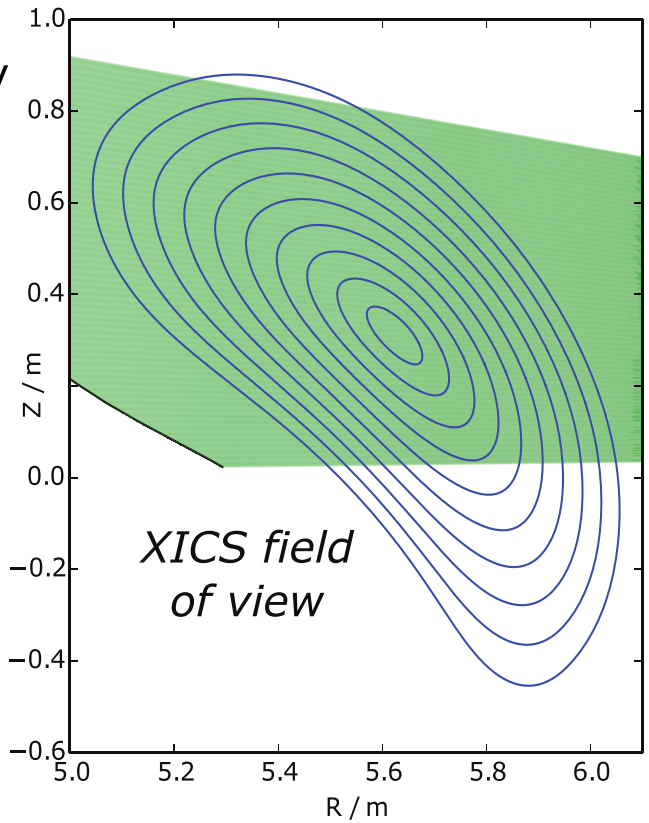

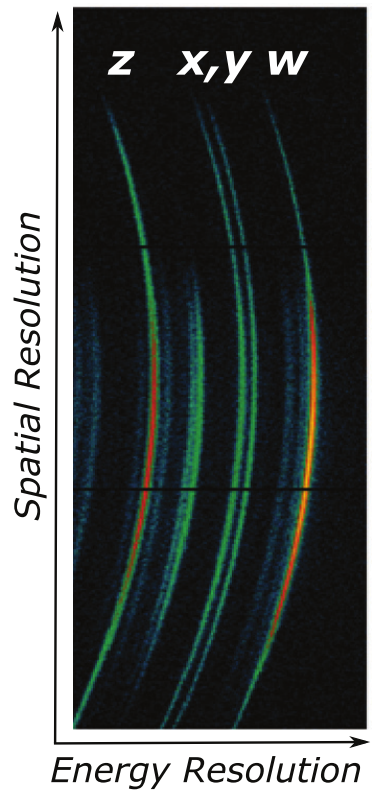

W-7X XICS system[2]

[1] Bitter *et. al*, RSI. **70**, 1999

[2] Figure reproduced from Langenberg *et. al*, NF **57**, 2017

Tungsten lines exist in CSXR spectral range

- Tungsten lines for W^{44+} and greater known to exist in .39-.4 nm
- However, an uncharacterized tungsten line $(W^{46+}?)^1$ exists near the 'X' Ar line
- Qualitatively known that high core T_e is necessary for significant emission

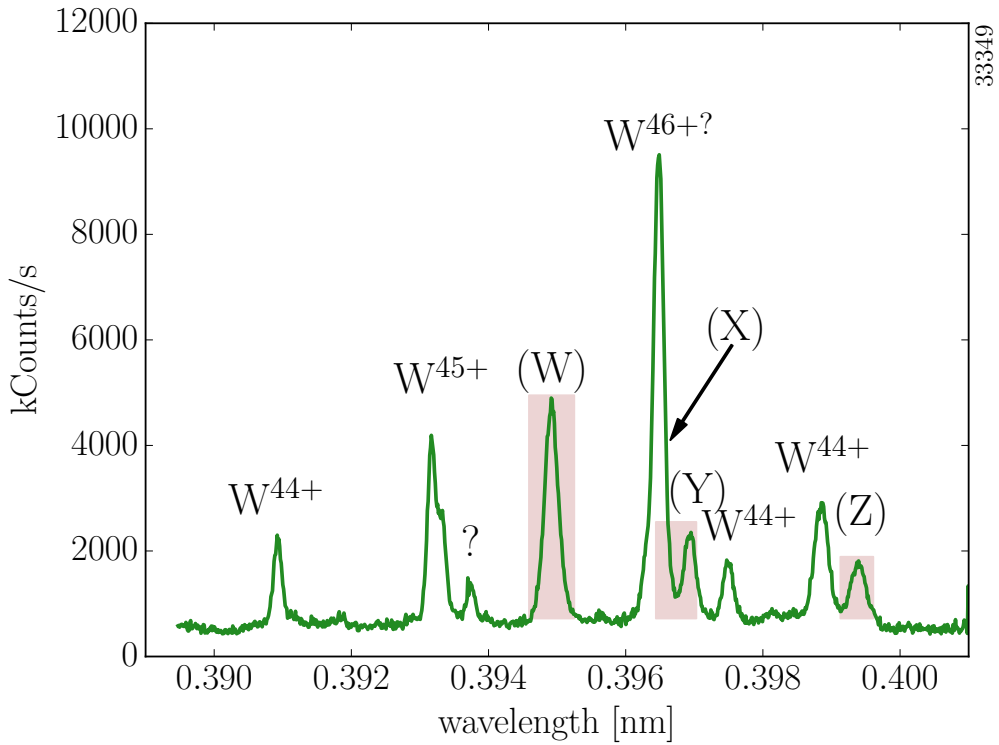

[1] M. Sertoli Thesis (LMU 2010)

New tungsten line opens possible physics experiments, new W measurements

- High T_e W line could be used elsewhere for single charge state, High-Z impurity transport studies
- Once understood, the absolute calibration could also be used as a tungsten measurements or for improving accuracy
- Goal is to relate CSXR to other W measurements through the tungsten concentration

Grazing Incidence (GI) spectrometer measures tungsten concentration

- The GI determines concentrations for low (~ 1 keV) T_e and higher (~ 4 keV) T_e from two distinct features

$$\langle c_W \rangle_l = \frac{I_{GI}}{I_{calc}(n_e, T_e)}$$

- c_W - tungsten concentration
- I_{GI} - Intensity of GI spectral feature
- $I_{calc}(n_e, T_e)$ - Expected intensity calculated from n_e, T_e profiles (with assumption about impurity density profile)

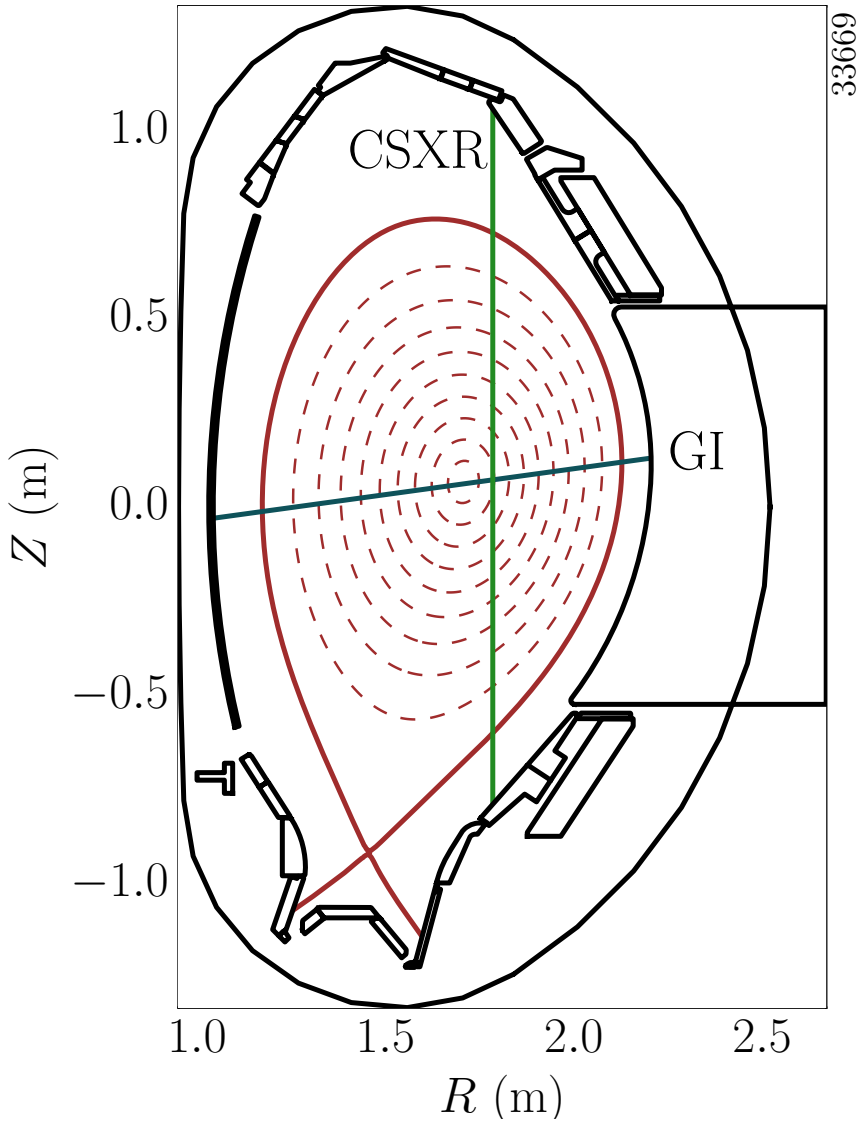

$I_{calc}(n_e, T_e)$ relies on fractional abundance of charge states

$$I_{GI} = \frac{G}{4\pi} \int n_e^2 c_W \, PEC(n_e, T_e) f_Z(T_e) dl$$

$$I_{calc} = \frac{G}{4\pi} \int n_e^2 \, PEC(n_e, T_e) f_Z(T_e) dl \; [1]$$

- G - sensitivity (with étendue)
- $PEC(n_e, T_e)$ - Photon Emissivity Coefficient
- $f_Z(T_e)$ - fractional abundance of charge state
- Remember $\rightarrow c_W = n_W / n_e$

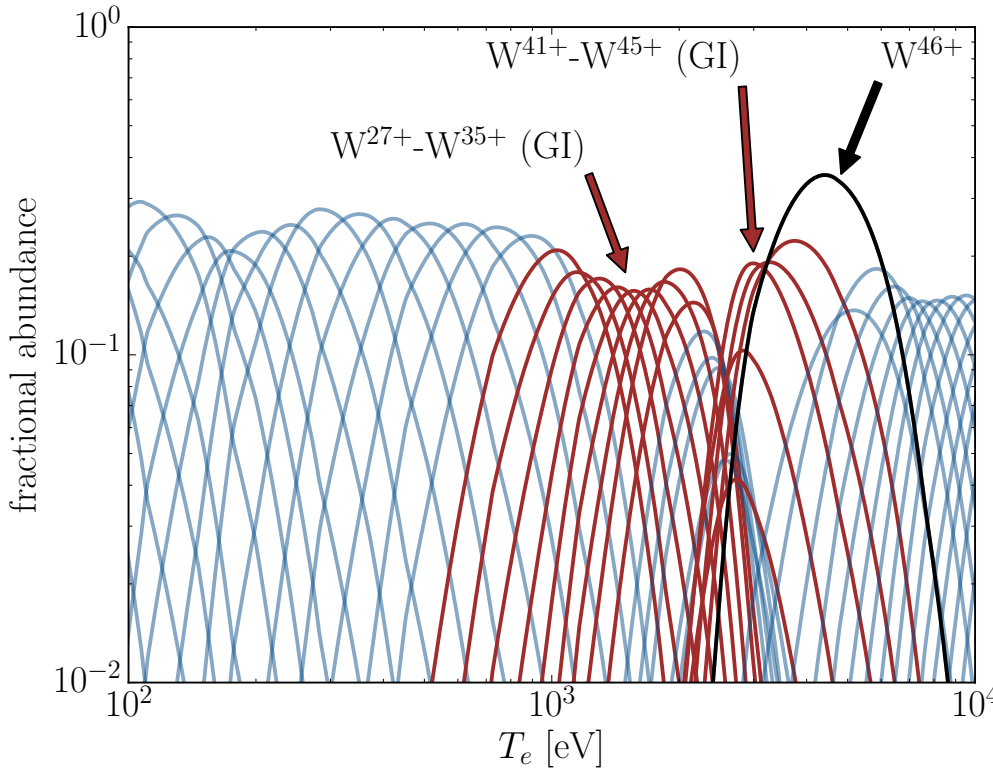

I_{CSXR} T_e dependence defined by the term: $PEC \cdot f_Z = \tilde{f}_Z$

[1] Adapted from Pütterich *et. al.* PPCF **50**, 2008

Solving for $\tilde{f}_Z(T_e)$ requires rethinking sightline measurements

- Values needed for calculating spectral intensity are spatial functions (of l), not functions of T_e
- Spatial sightline integral must be recast as a function of T_e to simply solve for $\tilde{f}_Z(T_e)$ (*e.g.* change $T_e(l)$ to $l(T_e)$)
- I_{CSXR} equation is recast w.r.t. T_e for tomography problem and discretized

$$I_{CSXR} = \frac{Gc_W}{4\pi} \int n_e(l)^2 \tilde{f}_Z(T_e(l)) dl$$

$$I_{CSXR} = \frac{Gc_W}{4\pi} \int n_e(T_e)^2 \tilde{f}_Z(T_e) \frac{dl}{dT_e} dT_e$$

$$I_{CSXR} \approx \frac{Gc_W}{4\pi} \sum_j n_e(T_{e,j})^2 \tilde{f}_Z(T_{e,j}) \Delta l(T_{e,j}) = \frac{Gc_W}{4\pi} \sum_j M_j \tilde{f}_Z(T_{e,j})$$

Matrix representation of $\tilde{f}_Z(T_e)$ constructs simplified inverse problem

$$\mathbf{M}_{ij} = n_{e,i}^2(T_{e,j})\Delta l_i(T_{e,j})$$

$$\vec{I}_{CSXR} = \frac{G}{4\pi}\vec{c}_W \circ \left(\mathbf{M} \cdot \vec{\tilde{f}}_Z(T_e)\right)$$

- $c_{W,i}$ is determined by GI spectrometer, for shot i
- M_{ij} developed from EQH shotfiles with CSXR sightline
- Same n_e and T_e profiles were used for original $c_{W,i}$ calculation

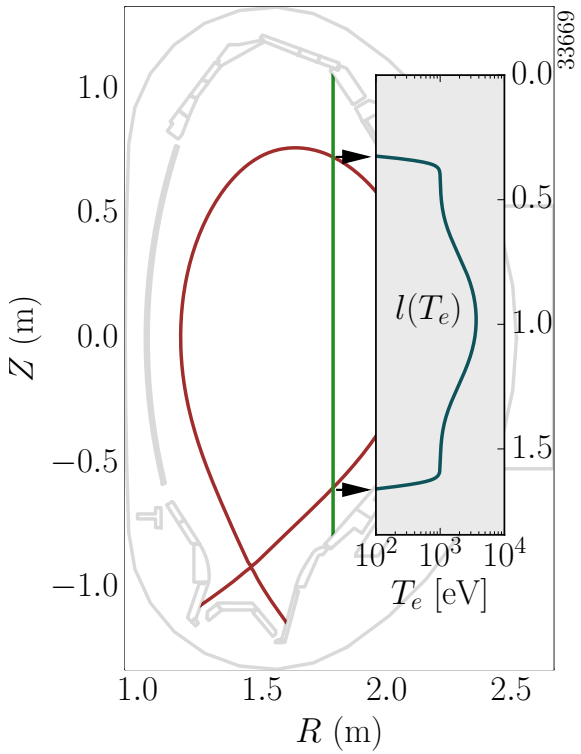

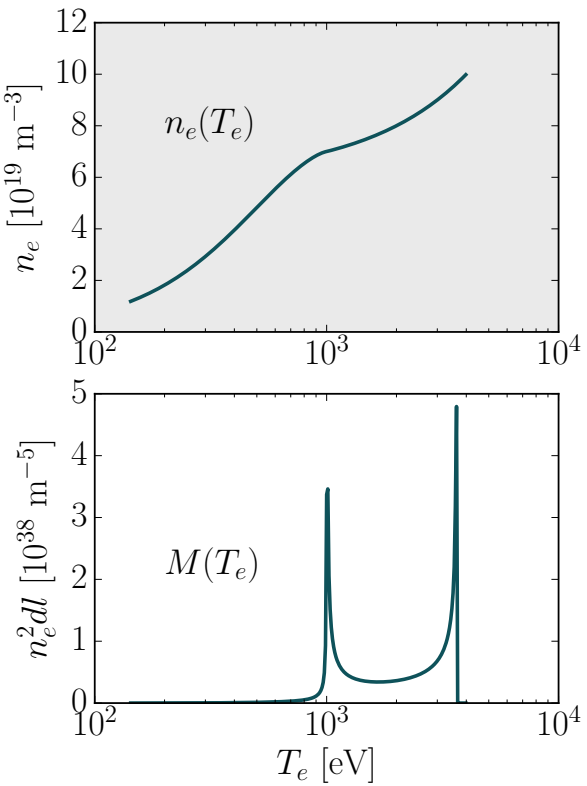

The simplified problem can be solved using the two spectrometers, Thomson profiles, and equilibrium data

Goal is to use varying T_e conditions to extract $\tilde{f}_Z$

- This linear integral problem in T_e is relatively ambiguous
- Comparisons of different T_e circumstances are needed to extract values
- Goal: Assemble $\mathbf{M}$ with different T_e conditions
- Similar methods would utilize W accumulation[1] to remove ambiguity $\rightarrow$ no inversion needed

Instead of specific plasma conditions to reduce ambiguity, this approach relies on large datasets (all data from 2014-2018).

[1] Pütterich *et. al.* PPCF **50**, 2008

Forward model provides insight on dataset limitations

- M, I_{CSXR} can be defined by the highest T_e along the sightline and histogrammed
- A general model of M can be combined with ADAS $\tilde{f}_Z$ values to create a forward model for comparison
- Fractional abundance of W^{45+} with a corresponding PEC best matches forward model
- Statisitical significance limited to range of data can be observed ($\approx$ 2-7 keV)

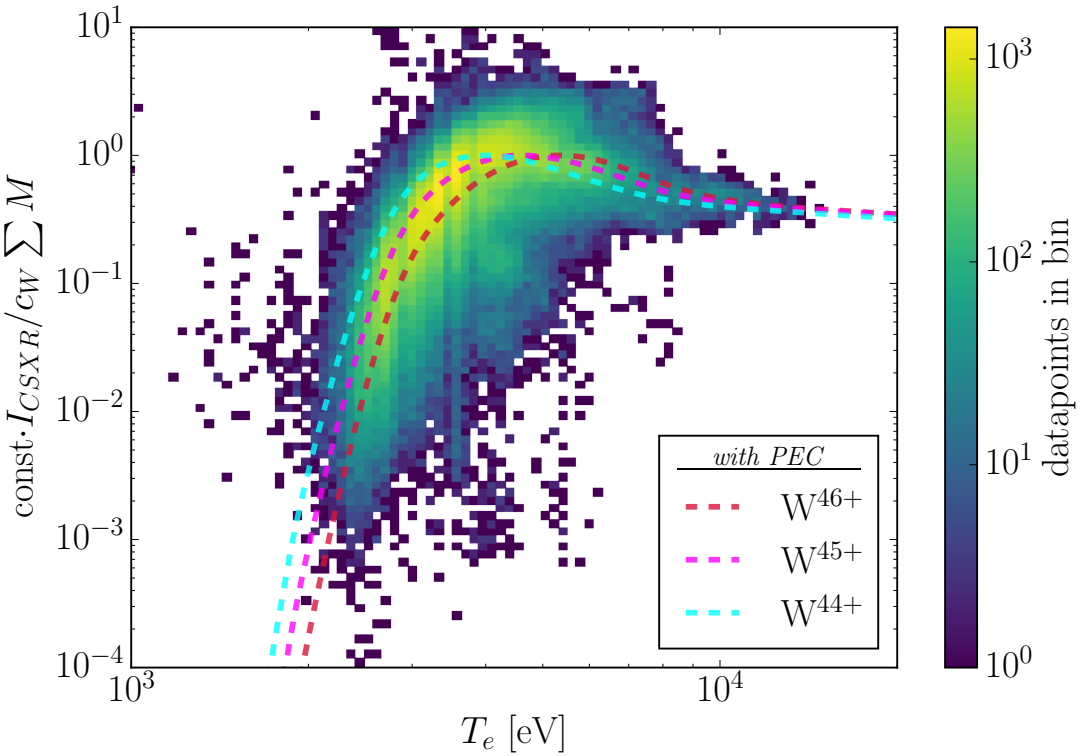

Shown data for 2016-2018, 100k points

Inversion result states line is W^{45+}

- Dataset separated into 2 (years 14-16 and 16-18), as fitting and cross-validation sets
- Optimal solution closely matches W^{45+}
- In total, over 300k spectra used
- Further smoothing is likely, errorbars must be first generated
- Shown solution minimizes $\left(\log(I_{CSXR}) - \log(c_W M \tilde{f}_Z)\right)^2$

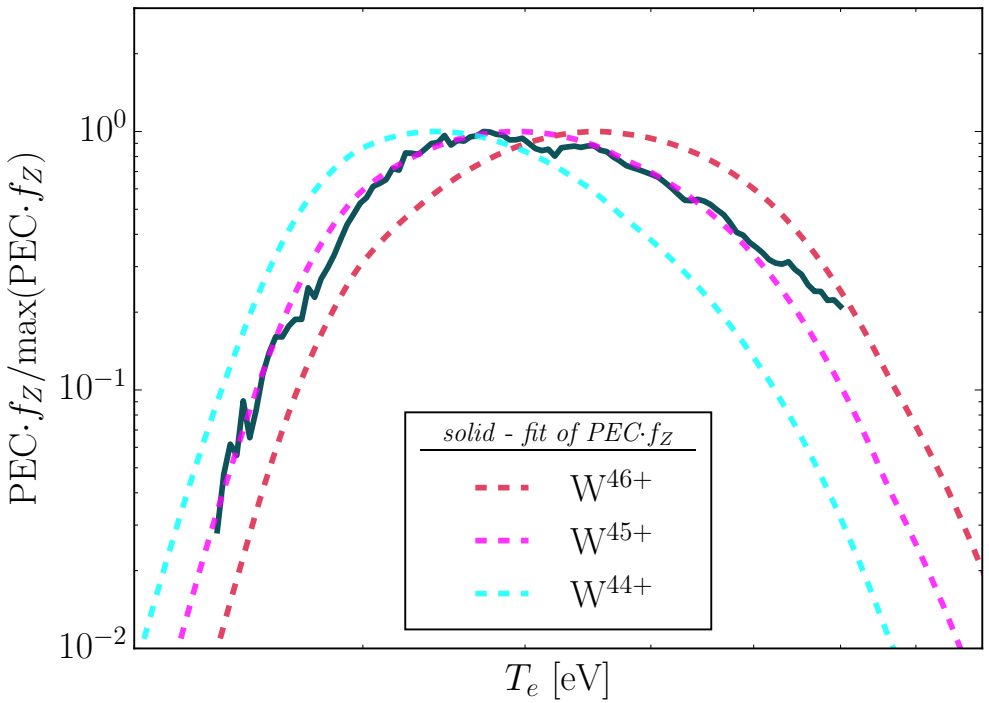

Conclusions and future work

- This work shows that the intense .39648nm tungsten line is W^{45+}
- The determination of error bars is required, and is not yet defined
- Next steps ideally would further study on EBITs/ or with codes for better characterization
- When understood, it could be used to do single charge state density profiles $\rightarrow$ precise tungsten transport
- High T_e nature makes use over wide r/a difficult on current devices
- Can now be used as another measure of tungsten density, possibly address in/out asymmetries on AUG

Spectral Fitting and GIW information

Table of fitted lines in CSXR spectra

- fitted 13 gaussians (peak, width and offset) with an overall baseline

λ [nm]	Element/charge	Used λ	Source
.39097	W^{44+}	.3909	J. Clementson *et. al.* Phys. Scr. **81**, 2010
?	?	.39316	-
.3933	W^{45+}	.39331	N. Tragin *et. al.* Phys. Scr. **37** 1988
?	?	.39374	-
.39490	Ar^{16+} ('W')	.39492	H. Bruhns, *et. al.* Phys. Rev. Lett. **99** 2007
?	?	.3955	-
.39636	W^{43+}	.3963	J. Clementson *et. al.* Phys. Scr. **81**, 2010
?	$W^{?+}$	.39648	-
.39649	Ar^{16+} ('X')	.39660	E. Källne *et. al.* Phys. Rev. A **28**, 1983
.39683	Ar^{16+} ('Y')	.39695	E. Källne *et. al.* Phys. Rev. A **28**, 1983
.3973	W^{44+}	.3975	N. Tragin *et. al.* Phys. Scr. **37** 1988
.39895	W^{44+}	.39887	J. Clementson *et. al.* Phys. Scr. **81**, 2010
.39934	Ar^{16+} ('Z')	.39943	E. Källne *et. al.* Phys. Rev. A **28**, 1983

Spectrum fitted using Python/C optimization of Maximum Likelihood

- The spectrum was fitted using Poisson random variable maximum likelihood estimation
- Minimization parameter was the negative log likelihood
- The L-BFGS-B algorithm was used due to fast optimization with minimal memory use
- This avoids problems often observed with low count-rate issues (harder to interpret fit quality)

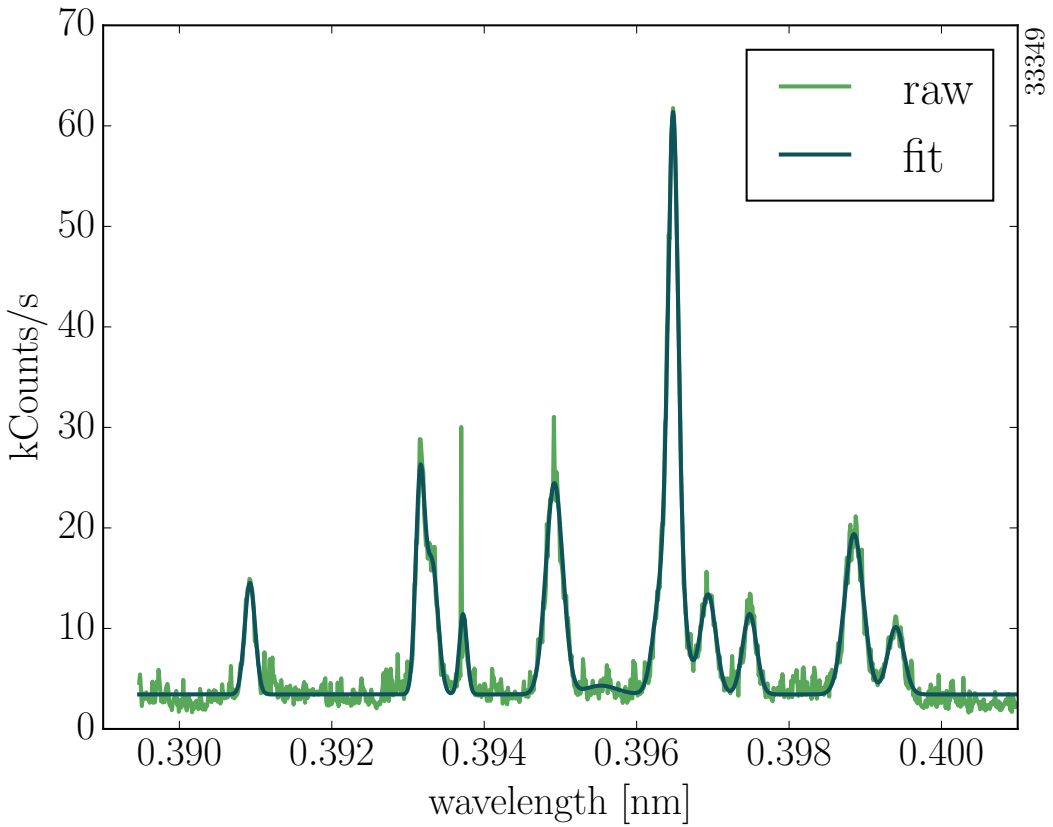

T_e, n_e profiles use parameterization from GIW c_W calculations

$$n_e(\rho) \approx (n_{e,core} - n_{e,ped})e^{-2\rho^2} + .5n_{e,ped}(1 + 80\tanh(.985 - \rho))$$
$$T_e(\rho) \approx (T_{e,core} - T_{e,ped})e^{-2\rho^2} + .5T_{e,ped}(1 + 60\tanh(.99 - \rho))$$

- Core and pedestal n_e, T_e values are fit non-linearly, and stored in GIW shotfile
- For consitency, they are re-used in this analysis
- On average are accurate, but hides profile shape behavior (*i.e.* variation from these shapes will induce errors)

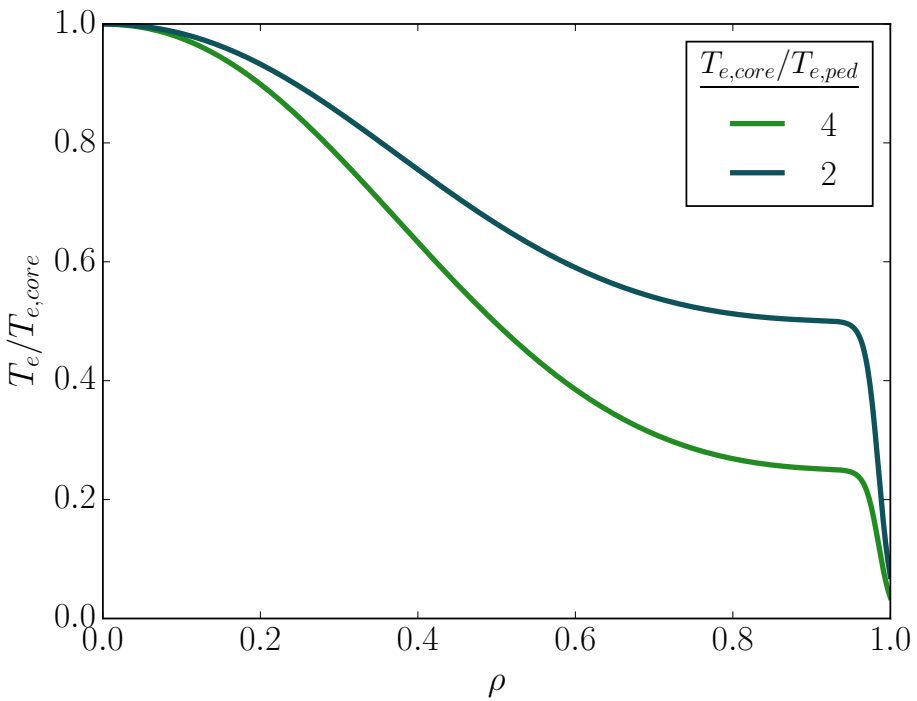

Forward Model

Forward model derivation

$$I_{CSXR} = \frac{G c_W}{4\pi} \sum_j M_j \tilde{f}_Z(T_{e,j})$$

$$\frac{4\pi I_{CSXR}}{G c_W \sum M} = \sum_j \frac{M_j}{\sum M} \tilde{f}_Z(T_{e,j}) = \sum_j \hat{M}_j \tilde{f}_Z(T_{e,j})$$

- We solve for a simplified $\hat{M}$ which is only a function of $T_{e,max}$, this assumes a low pedestal temperature and rigid profile shapes. This is knowingly approximate
- The $I_{CSXR}/c_W \sum M$ term is histogrammed based on the peak observed sightline temperature $T_{e,max}$.
- Various $\tilde{f}_Z$ can be applied in order to see which minimizes a log squared objective function.

Model of M allows for understanding of dataset

- A simple normalized model M is used to represent the sightline in T_e space
  - $T_{e,ped}$ - fixed value of 600eV (value is relatively unimportant)
  - $T_{e,max}$ - Maximum temperature for sightline
  - λ - decay length
  - a - baseline value
- This function can be used to generate forward models, due to the simplification to 4 variables

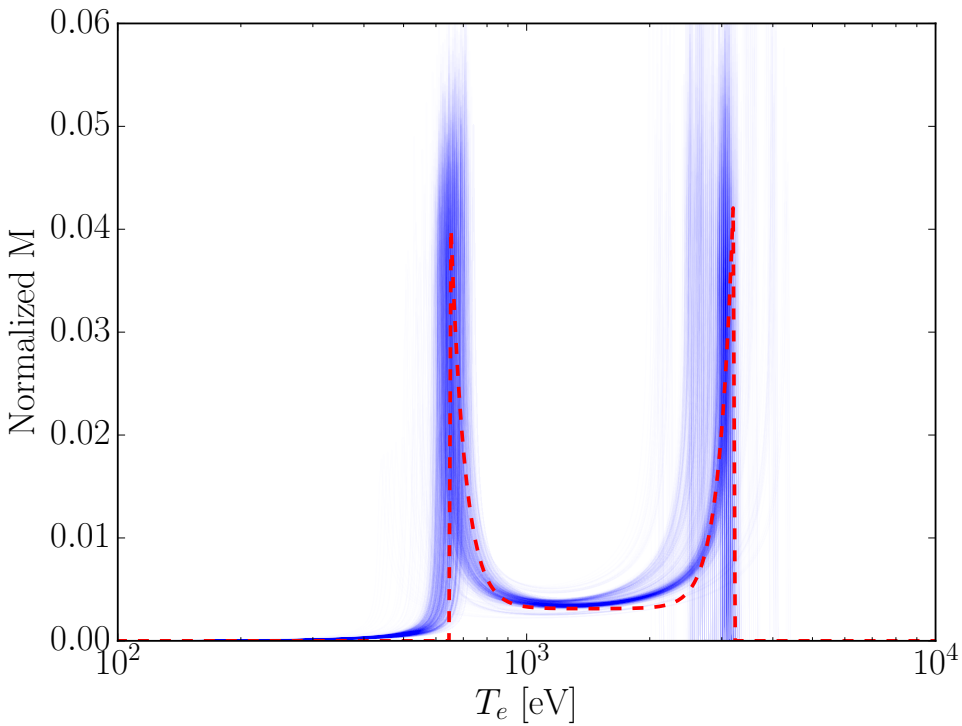

$$\hat{M}(T_e) = \frac{a + \left(\frac{T_{e,ped}}{T_e}\right)^{1/\lambda} + \left(\frac{T_e}{T_{e,max}}\right)^{1/\lambda}}{\sum_{j=T_{e,ped}}^{T_{e,max}} a + \left(\frac{T_{e,ped}}{T_j}\right)^{1/\lambda} + \left(\frac{T_j}{T_{e,max}}\right)^{1/\lambda}}$$

Model $\hat{M}$ reasonably describes M

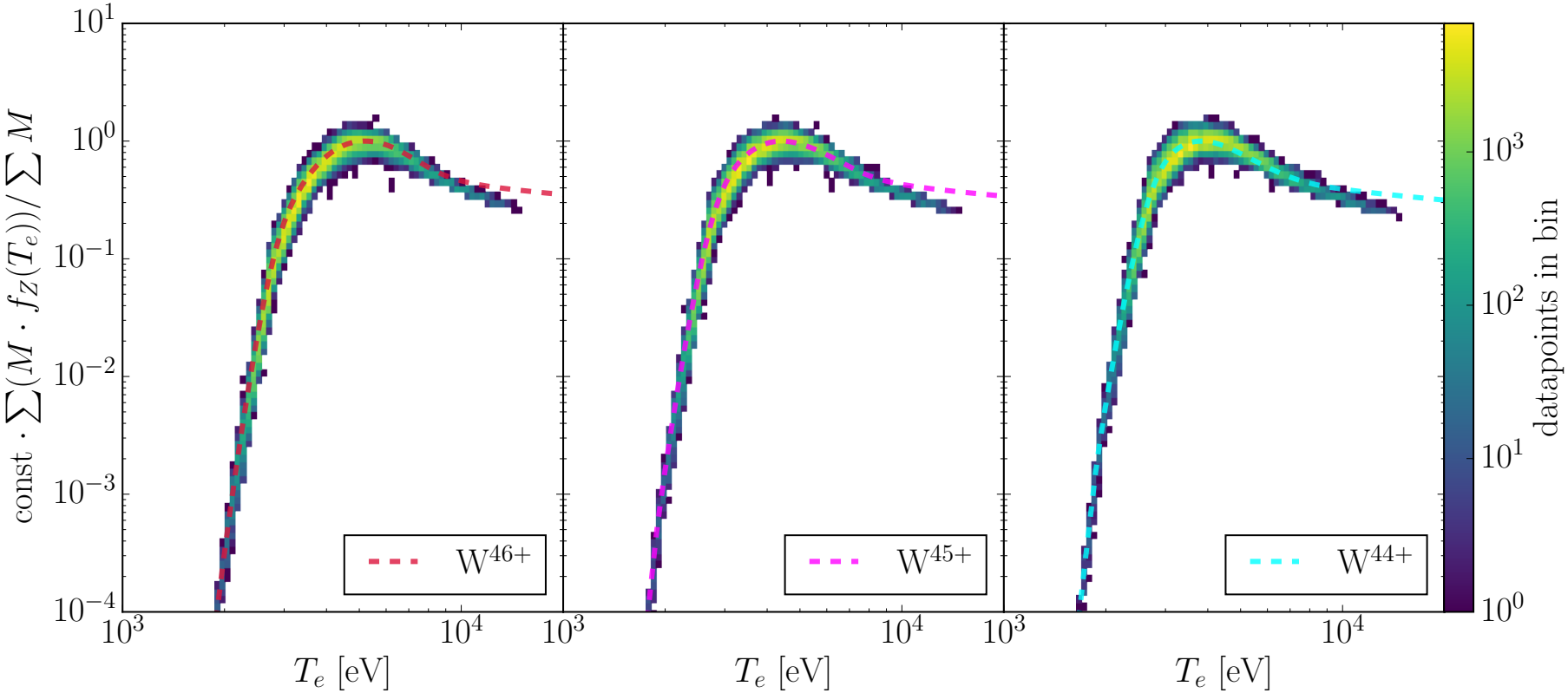

the model function $\sum \hat{M} f_Z(T_e)$ is compared to a heat map of experimental $\frac{\sum M f_Z(T_e)}{\sum M}$ for various charge states

Expected I_{CSXR} can visualize data variance as a function of $T_{e,max}$

- Data and forward model can be compared for total intensity as a function of $T_{e,max}$ (see equation)
- This is a powerful tool to understand dataset dependencies/limitations
- At lower T_e, I_{CSXR} is dominated by the rise in $f_Z(T_e)$
- At higher T_e, peak emission region moves off-axis and emitting region shrinks

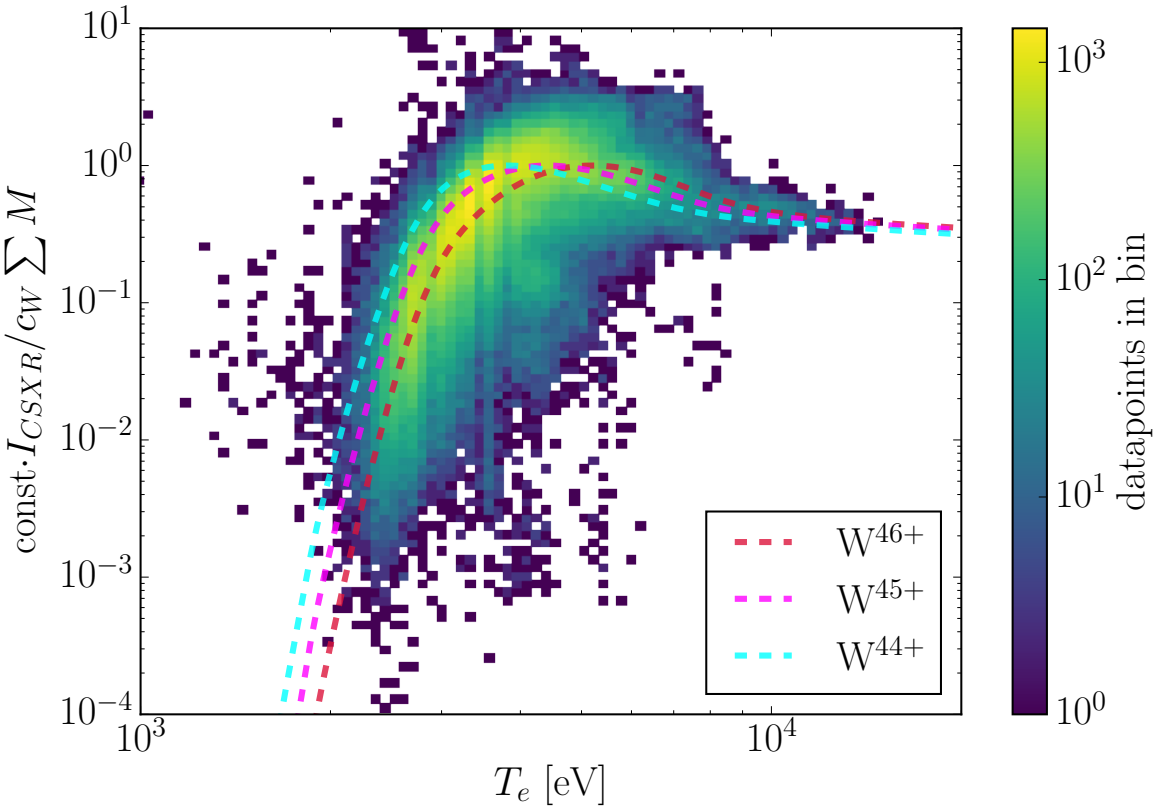

$$\sum_j \hat{M}(T_{e,max}) f_Z(T_{e,j}) \propto \frac{I_{CSXR}(T_{e,max})}{c_W \sum_j M(T_{e,j})}$$

Photon Emissivity Coefficient modifies forward model projections

- Original work assumed that the Photon Emissivity Coefficient (PEC) was a constant
- It is actually also a function of n_e and T_e, and will impact forward model
- All curves relatively similar, with 1 order of magnitude variation across T_e range
- Data taken from ADAS for highest emitting lines in .38-.41 nm wavelength range

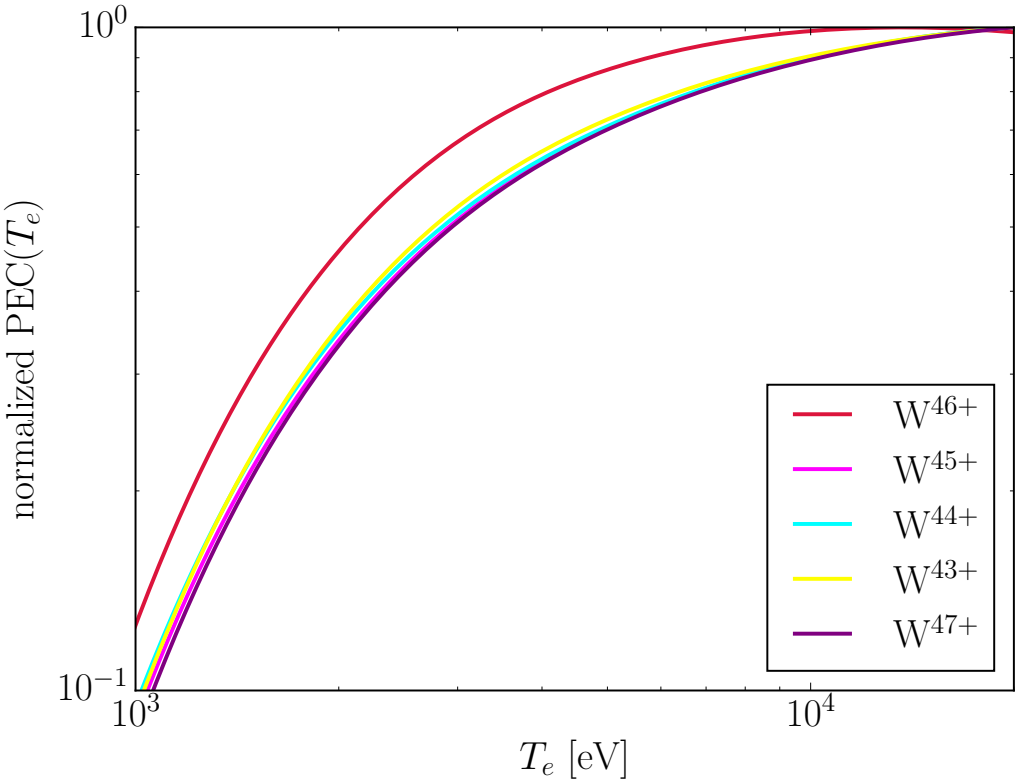

Forward model fits data better with non-constant PEC

- As PEC curves were monotonically increasing, it serves to shift modelled data to higher T_e
- The order of magnitude change in PEC shifts data only slightly, as change in f_Z is greater
- Peak of model also shifts slightly in all cases to slightly higher T_e

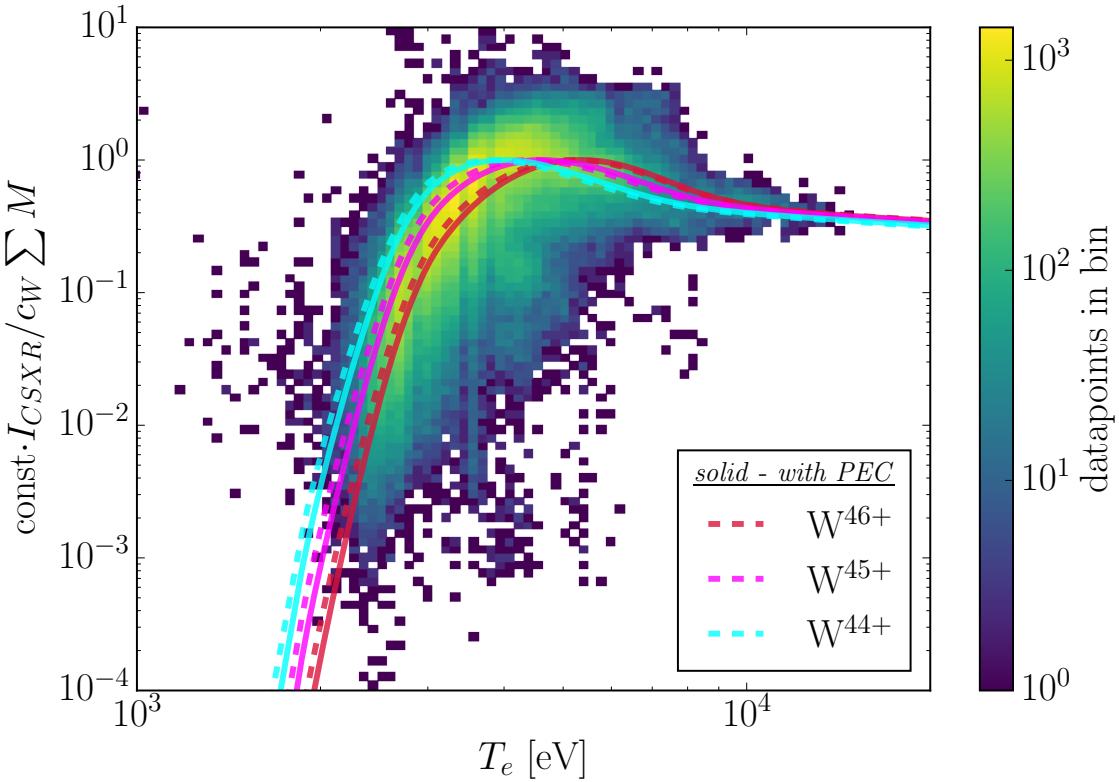

Forward model fits to W^{45+} with PEC

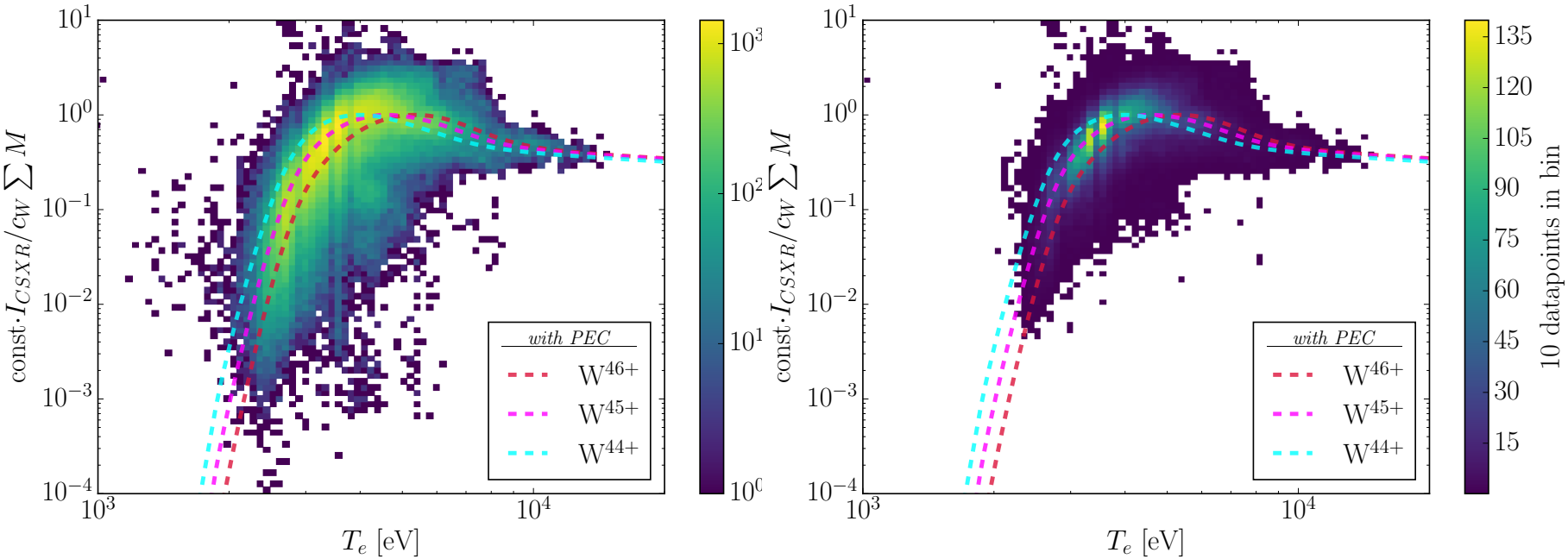

- Both plots show the PEC solutions with a linear and logarithmic color scheme (linear with lower cutoff of 100)
- Across electron temperatures with substantial data the best fit is W^{45+} with PEC
- At temperatures below 2 keV, c_W dataset is limited and distorts T_e dependence

Forward model R^2 shows line is W^{45+}

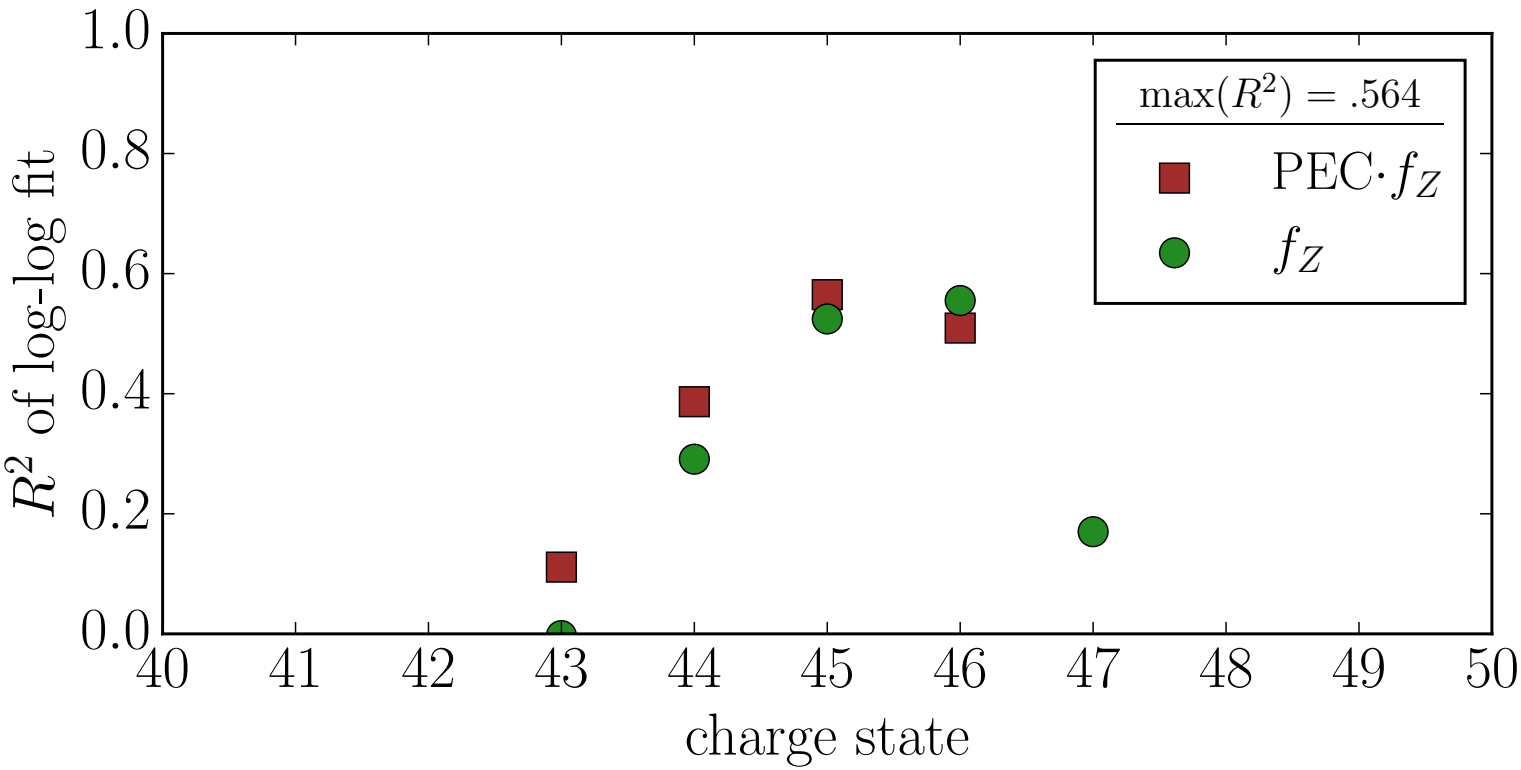

- While fit is non-linear (due to $\hat{M}(T_{e,max})$), we can use the R^2 as a general rule-of-thumb for goodness-of-fit
- Forward model contains highest values of R^2 for W^{45+} with PEC
- R^2 values for other charge states are negative

AUG Data Characteristics

Forward model suggests certain dataset issues

- Forward model simplifies data for rough understanding of dataset peculiarities
- Variation in data suggests solving inversion by minimizing $\sum(\log(\hat{X}_i) - \log(X_i))^2$
- This is true due to the ratio nature of the fitted data, and the associated error behavior
- Limitations in the dataset in T_e suggests a range of validity (2.3-7keV)

Known data with forward model helps to understand precision of data

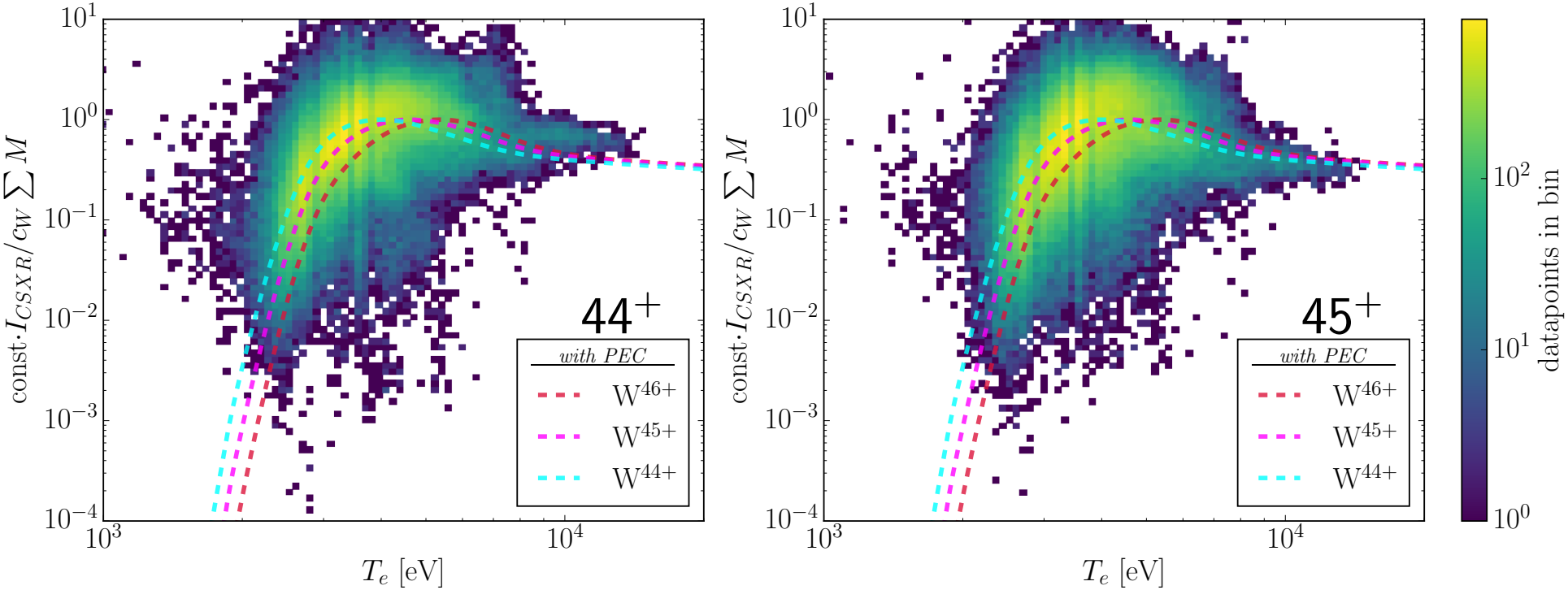

Using two lines of known charge state, significantly larger 'noise' in data is observed due to lower signal strengths.

Note: Only core concentration used for comparison

Noise for $T_e < 2$ keV suggests not using continuum c_W

- The GI measures a 'low T_e' - continuum c_W (top) and 'high T_e' - lines c_W (bottom)
- Limitations in the GI measurements limit 'high T_e' c_W range (> 2 keV)
- Larger variance in 'low T_e' data is due to larger physical separation (emission from largely different ρ)
- Forward model suggests use of only line radiation for analysis (as data < 2 keV is very noisy)
- However, similarity in trends gives confidence in analysis approach

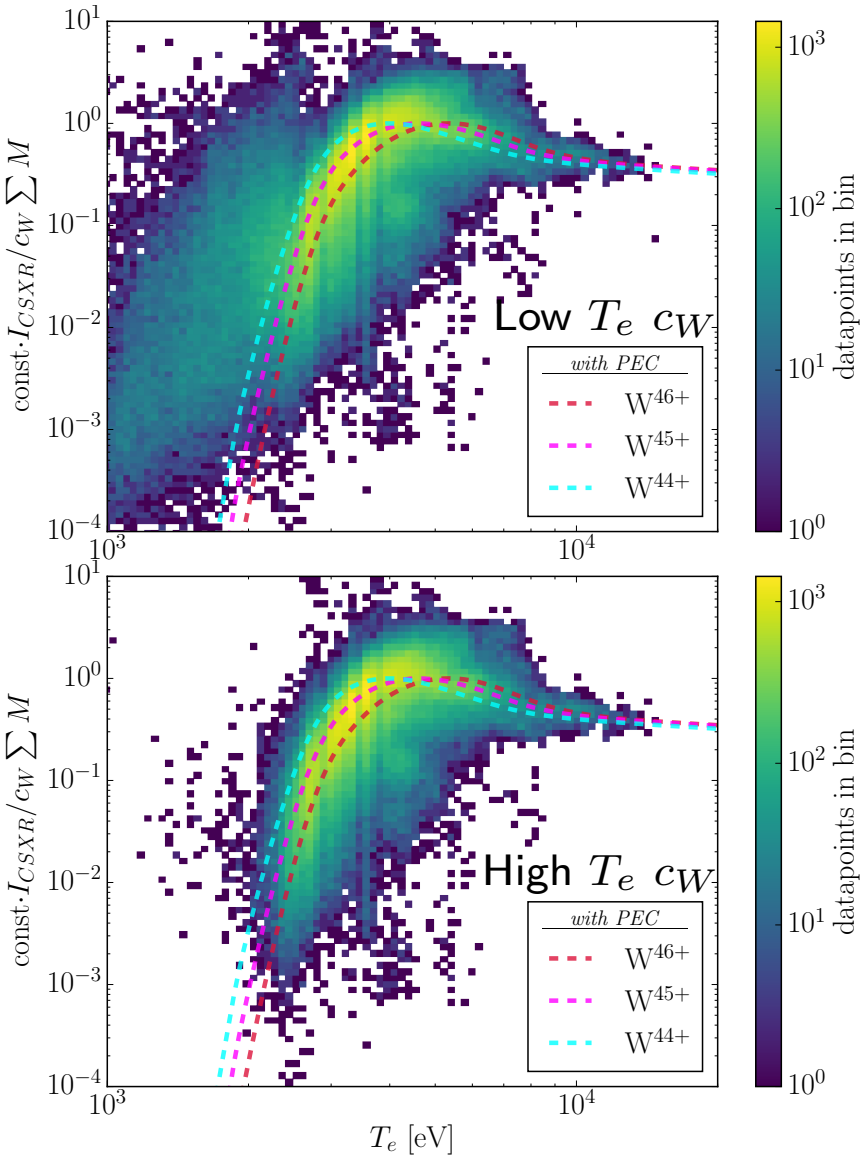

Least square methods can be biased estimators of T_e dependence

- Least squares methods assume homoscedasticity with a normal error distribution
- The forward model shows significant variation in σ^2 (*i.e.* significant heteroscedasticity)
- Validity of inversion will be checked across the region of relative homoscedasticity in T_e ($\approx$2-7 keV)
- Inversion approach- Treat each T_e as an independent variable, allowing for heteroscedasticity

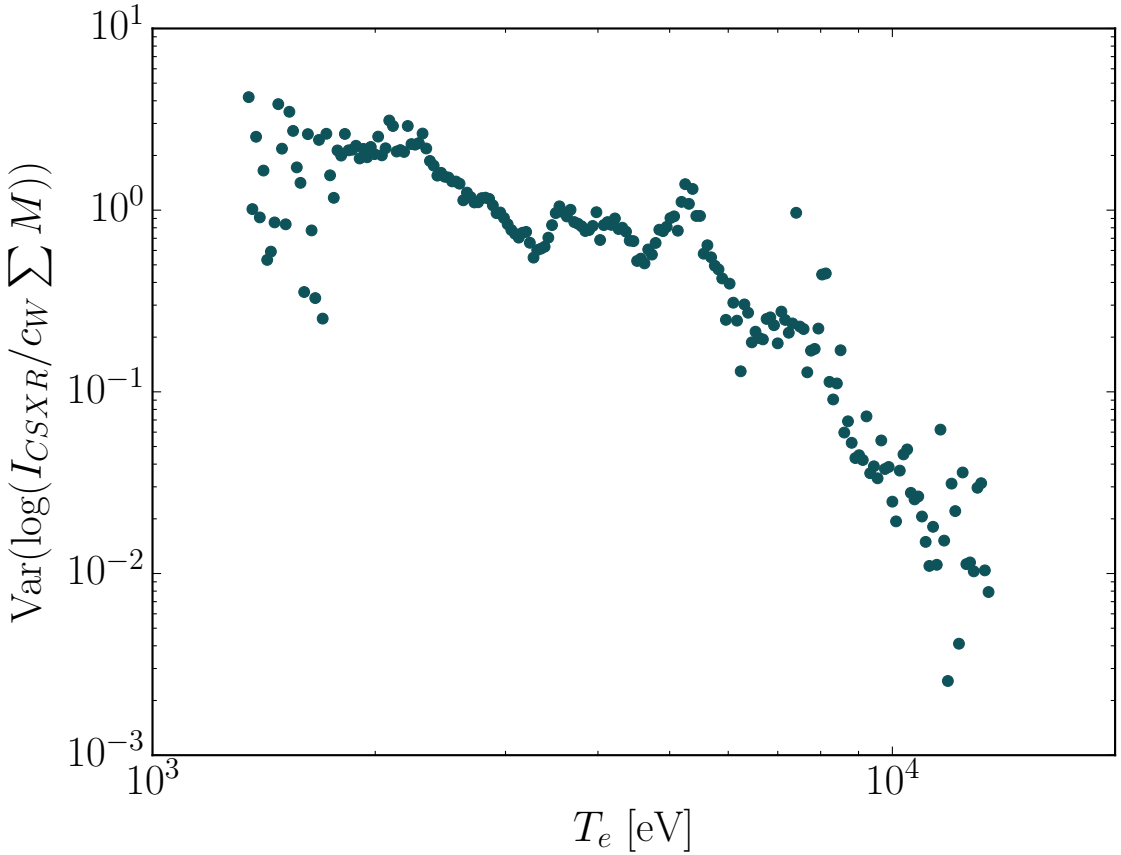

Significant variation seen in I_{CSXR}, c_W, and $\sum M$

- Shown on right is the average value of various parameters used for calculating the y-axis
- Even though I_{CSXR} count rates are Poisson distributed, most data has sufficient count rate to assume normal-like error probability distributions
- High value T_e data (> 7 keV) comes from a singular experiment (low n_e, high c_W, high I_{CSXR})
- Density trend ($\sum M$) suggests cutoff at $T_e < 2.3$ keV

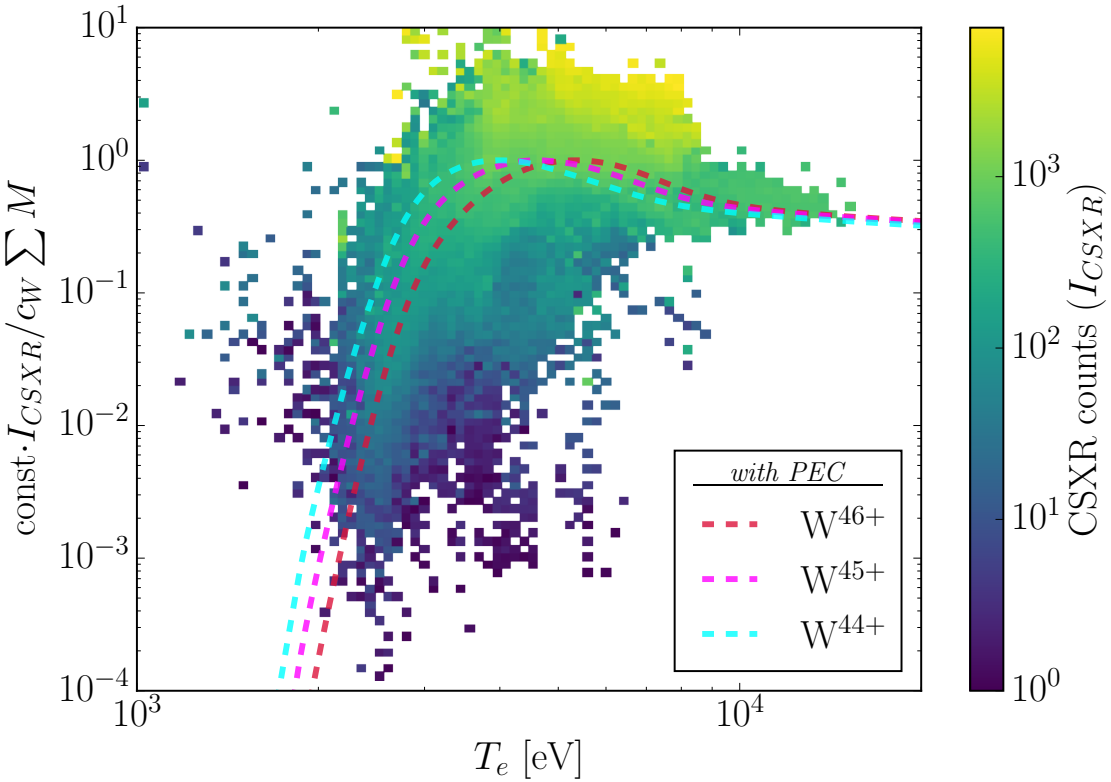

Significant variation seen in I_{CSXR}, c_W, and $\sum M$

- Shown on right is the average value of various parameters used for calculating the y-axis
- Even though I_{CSXR} count rates are Poisson distributed, most data has sufficient count rate to assume normal-like error probability distributions
- High value T_e data (> 7 keV) comes from a singular experiment (low n_e, high c_W, high I_{CSXR})
- Density trend ($\sum M$) suggests cutoff at $T_e < 2.3$ keV

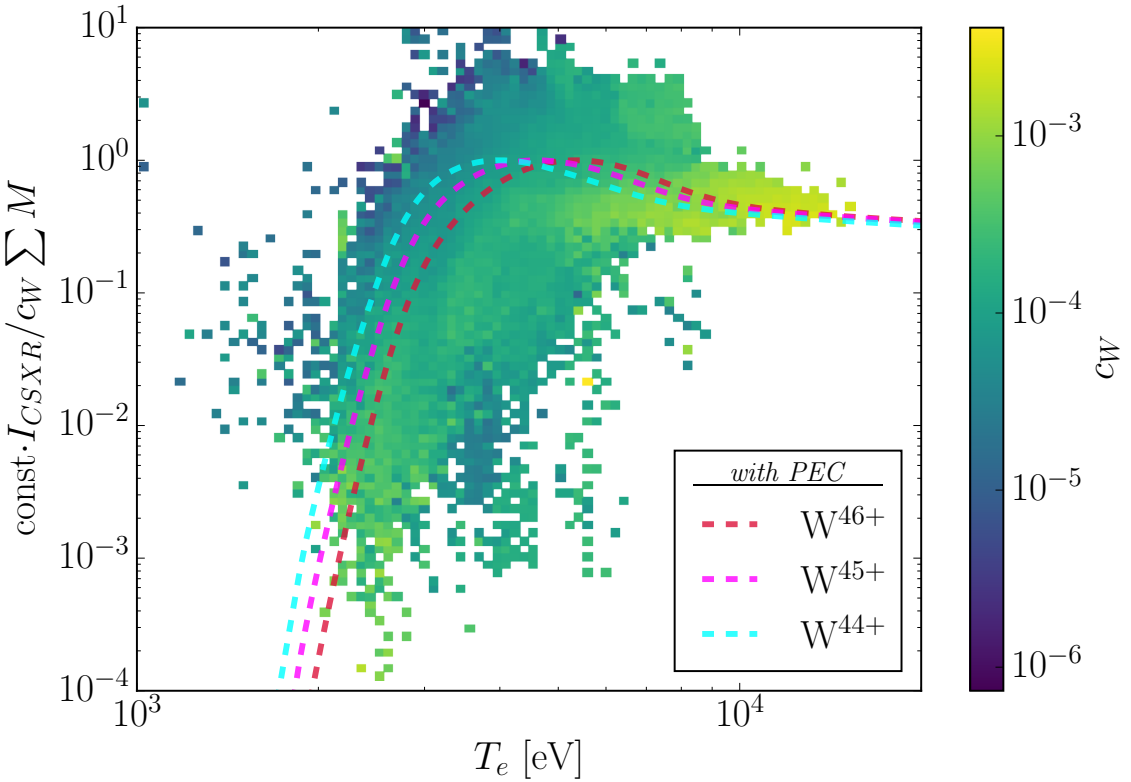

Significant variation seen in I_{CSXR}, c_W, and $\sum M$

- Shown on right is the average value of various parameters used for calculating the y-axis
- Even though I_{CSXR} count rates are Poisson distributed, most data has sufficient count rate to assume normal-like error probability distributions
- High value T_e data (> 7 keV) comes from a singular experiment (low n_e, high c_W, high I_{CSXR})
- Density trend ($\sum M$) suggests cutoff at $T_e < 2.3$ keV

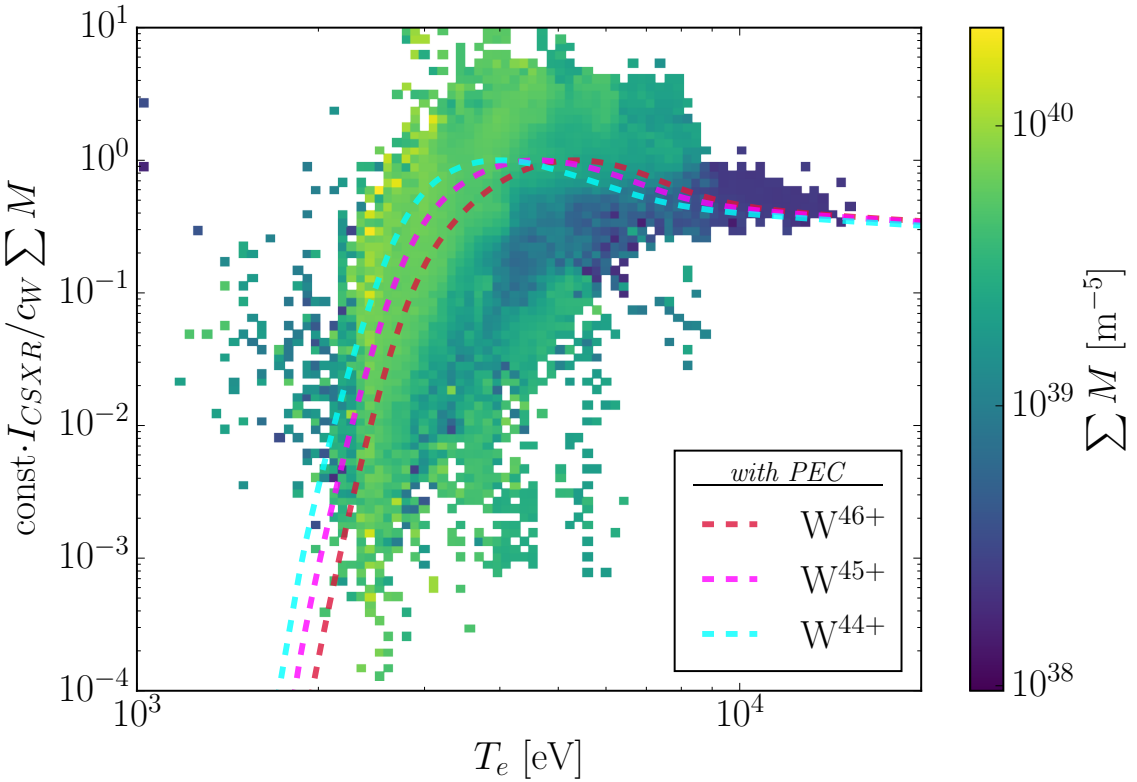

Log-normal fitting

Log-normal distribution poorly models line strength dynamics

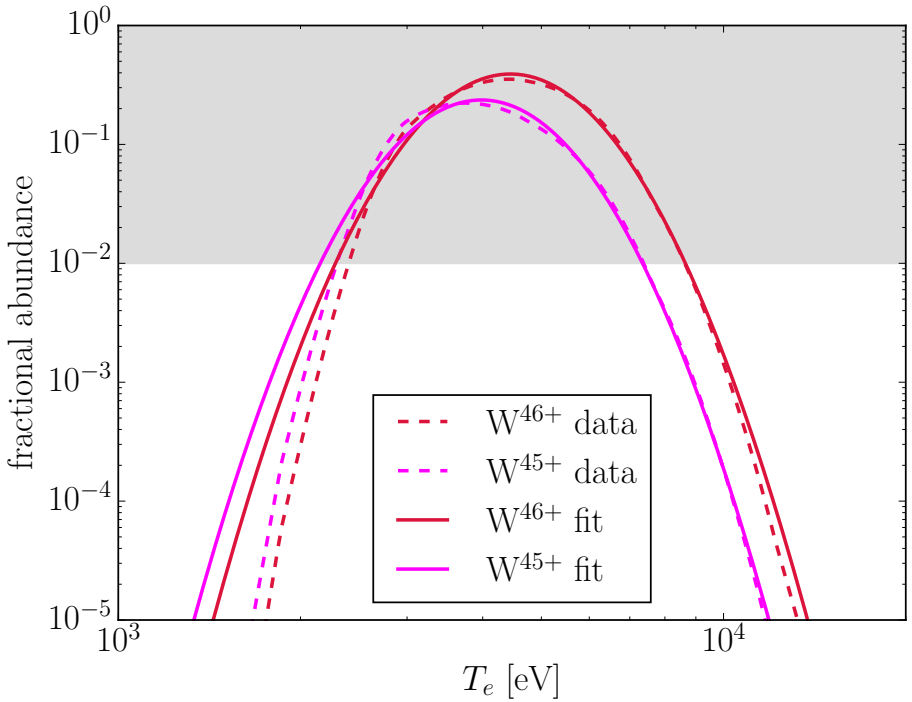

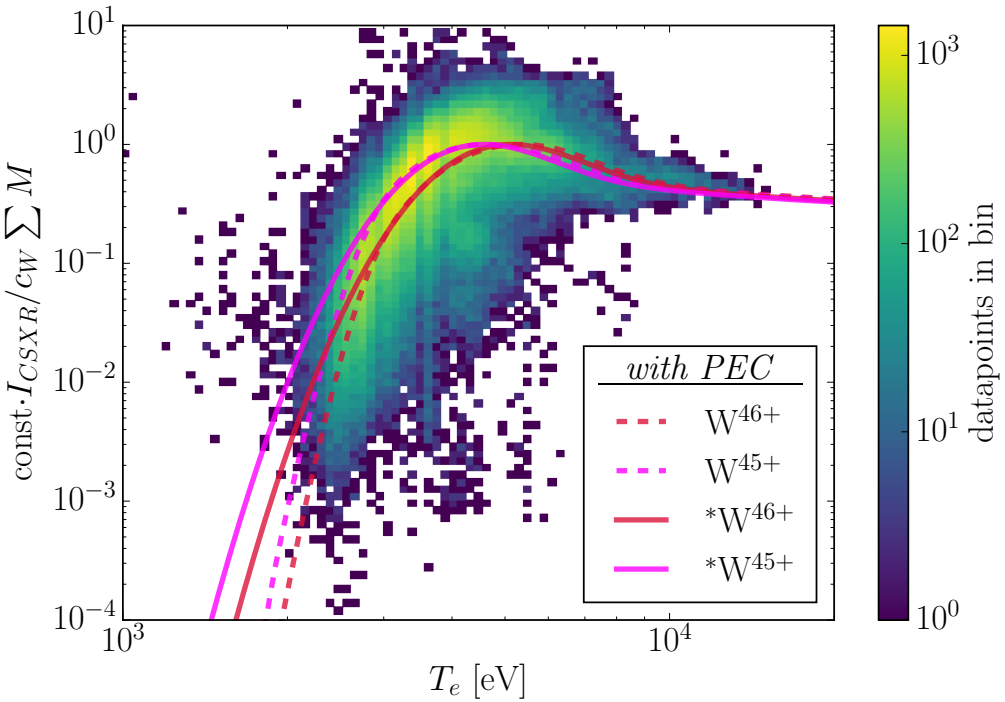

- Fractional abundance (from Pütterich *et. al.* 2008) is fit with a parabola in log-log space (*i.e.* log-normal distribution)
- Certain ranges are fit (shown in gray), offsets and widths between W^{45+} and W^{46+} are not accurately captured

Log-normal distribution poorly models line strength dynamics

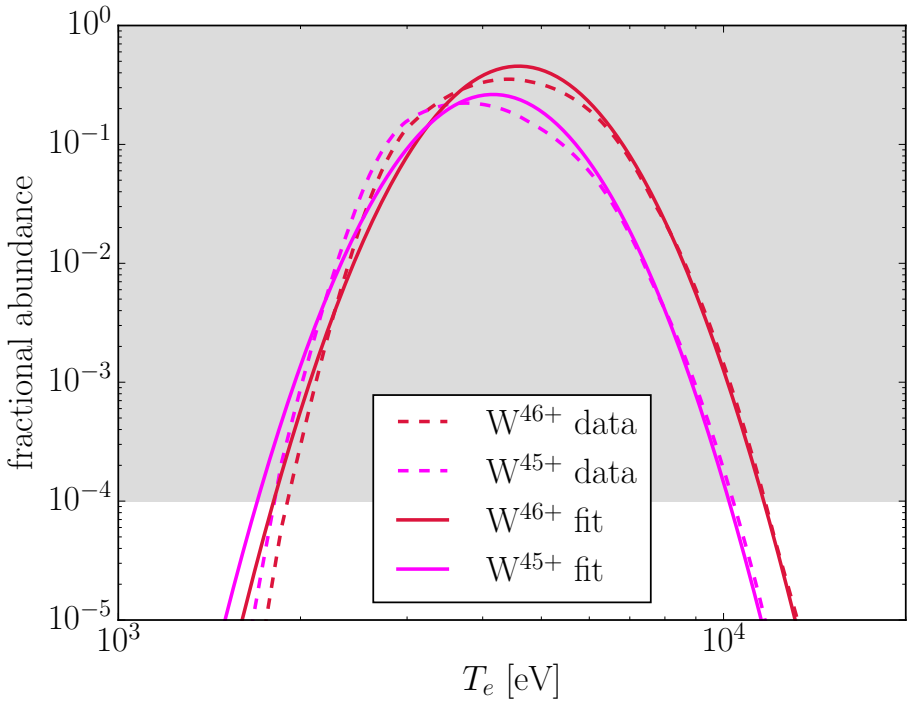

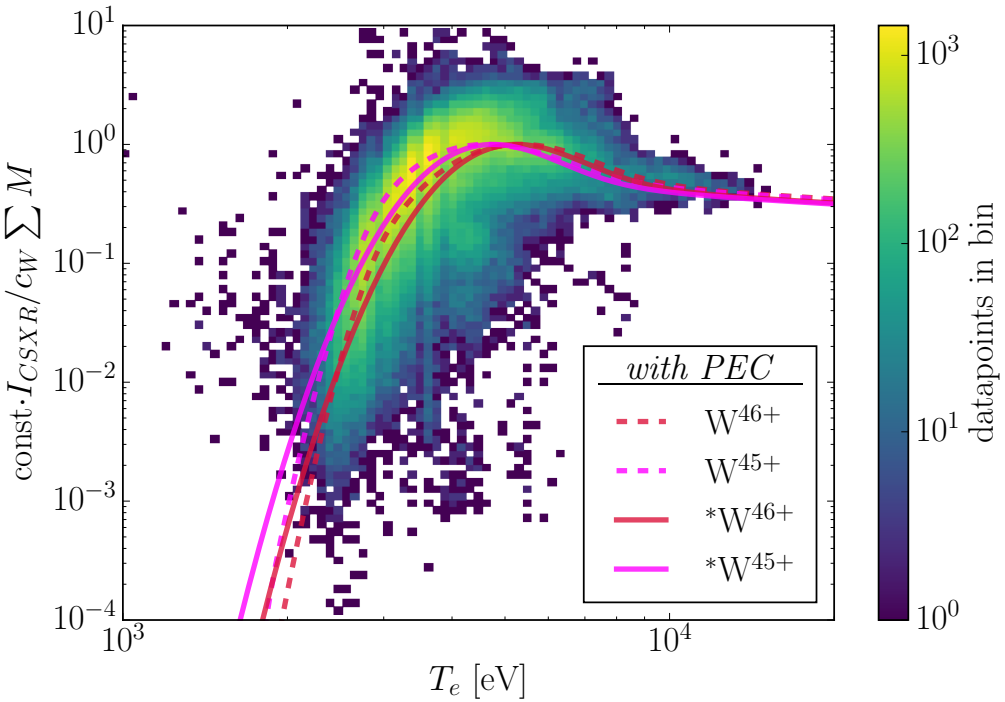

- Fractional abundance (from Pütterich *et. al.* 2008) is fit with a parabola in log-log space (*i.e.* log-normal distribution)
- Certain ranges are fit (shown in gray), offsets and widths between W^{45+} and W^{46+} are not accurately captured

Inversion results

Solving for $f_Z(T_e)$ is a classic ill-posed linear inverse problem

- This and other tomography problems are classified as Fredholm integration equations of the first kind

$$I(t) = \int_a^b M(t,s) f(s) ds$$

where $M(t,s)$ is the kernel, $I(t)$ is the data, with unknown $f(s)$

- These problems are ill-posed but can yield 'reasonable' solutions with additional constraints/ conditioning
- We know that $f_{\mathrm{CSXR}}(T_e)$ is positive and 'smooth' (should resemble theoretical predictions of $f_Z(T_e)$)

GI c_W values used for analysis are only correlated to c_W of tungsten CSXR lines

- The c_W from the GI spectrometer are possibly from other charge states (*i.e.* other regions of plasma)
- Tungsten concentration is a model for the radial profile of tungsten, and is valid as a local measurement
- Thus, $c_{W,\mathrm{GI}}$ is an 'unreliable narrator' and is likely to contain systematic bias/ variance for determining $c_{W,\mathrm{CSXR}}$

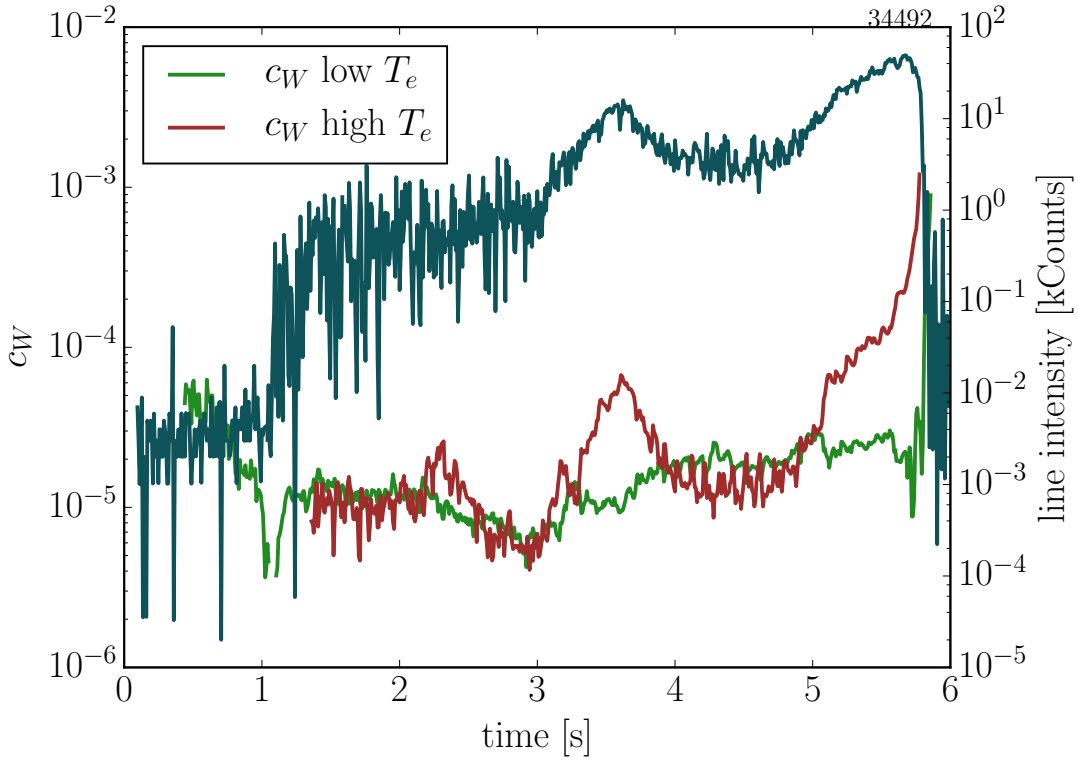

Cross Validation dataset generated from 2014,2015 campaigns

- Regularization introduces a free parameter λ which addresses overfitting/noise
- This free variable must be determined in an unbiased manner (cross-validation)
- A secondary dataset, from the 2014 and 2015 campaigns, was generated to determine this value
- Discrepancies between the two sets comes from changes in detector sensitivity, aquisition time, etc.
- Over 200k points

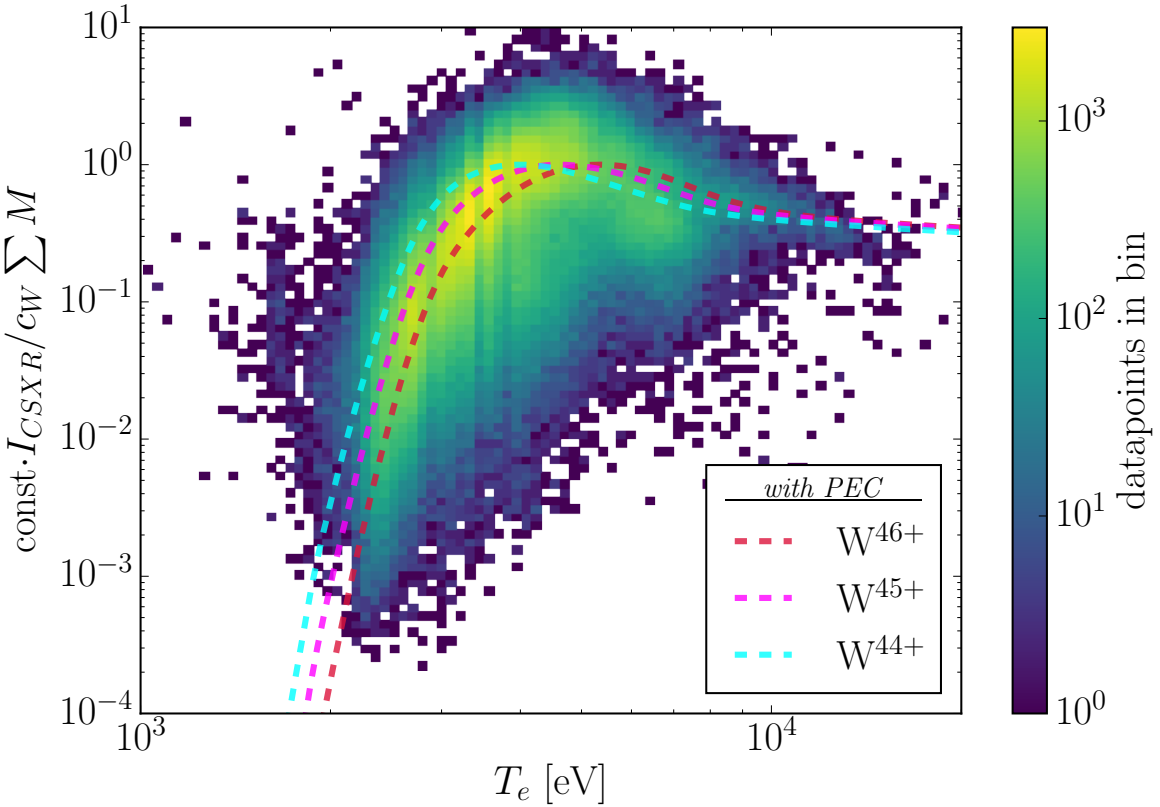

Properties of $\tilde{f}_Z$ used to inform regularization

- The parabolic-like nature of the $\tilde{f}_Z$ suggests a relatively invariant second derivative w.r.t T_e
- 'Smooth nature' suggests that overfitting must be minimized as much as possible
- A normal regularizer (CV λ), and a second derivative regularizer ($\partial^2 f_Z$ λ) were both cross-validated on the dataset
- Results show similar results, with differences at high T_e
- NOTE: data non-linearly fit (due to size), but cross-validated solutions were the same regardless of starting condition

Cross Validation (CV) shows optimum λ

- Regularization introduces a free variable which must be optimized (λ)
- Cross validating against the 2014-2016 data shows that some regularization is optimal
- This effort negates the noise-amplifying nature of the inversion, preventing overfitting
- In this case: optimal $\lambda = 4149.5$, however shallow variation indicates significant variation in CV dataset

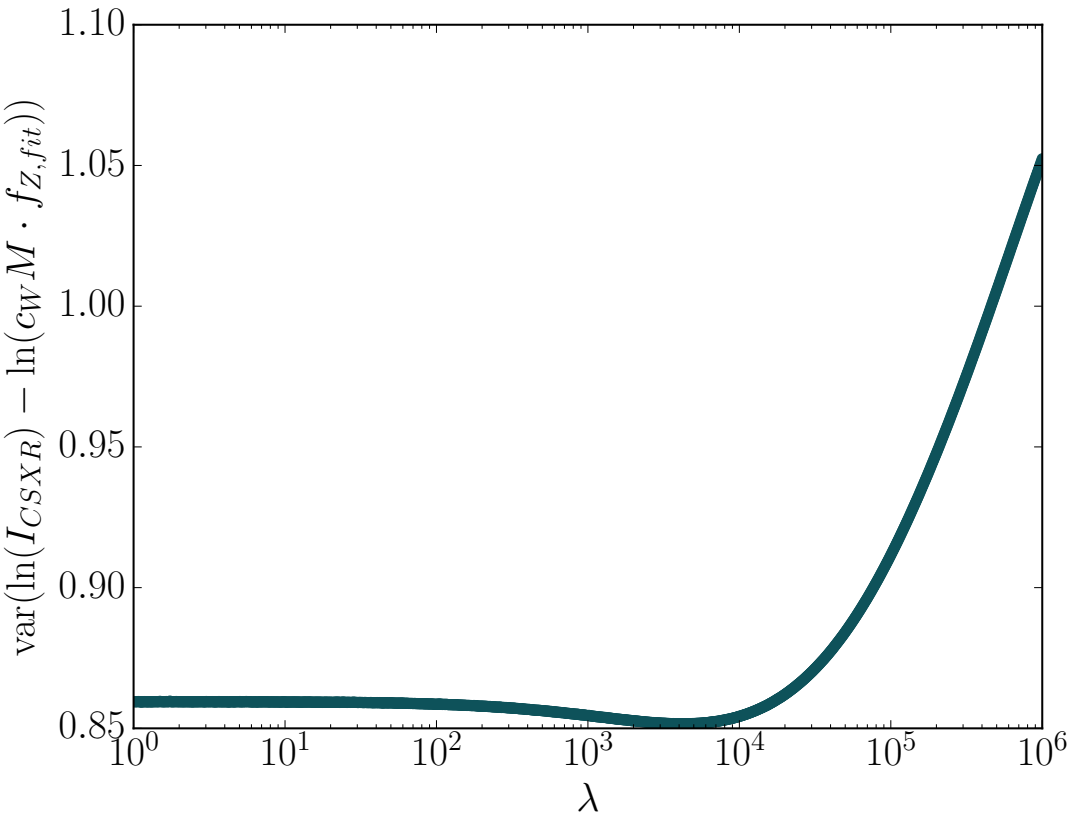

Cross-Validated inversion result also states unknown line is W^{45+}

- Results closely follows the observed $PEC \cdot f_Z$ of the W^{45+} charge state
- Offset in green is false, due to spurious noise and the nature of the normalization
- CV result is still 'noisy' but likely due to expected variation in both datasets (and within errorbars)

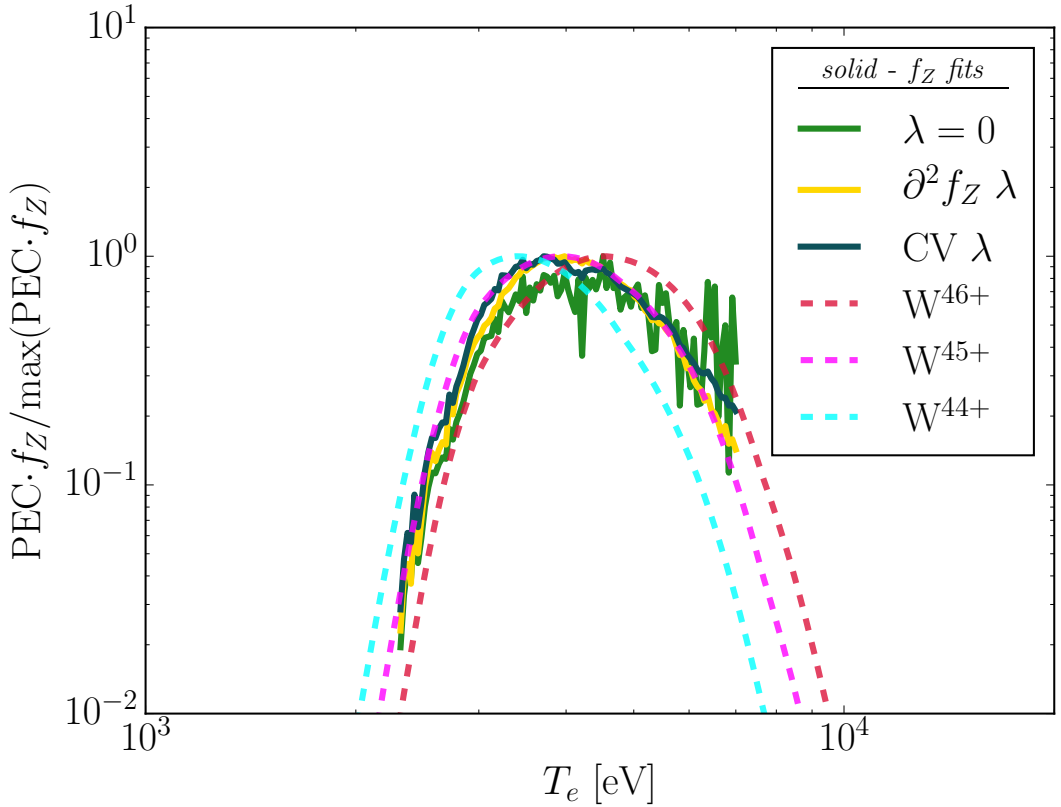

Inverted Model R^2 shows line is W^{45+}

- Model assumes each time point is an independent normally distributed variable.
- However, the comparison is not truly a 'fit' to the data but a comparison (invalidating the R^2, use as a rule of thumb)
- Result is clearer in comparison to forward model prediction